

A CALCULATION OF SPHERE-PLANE FIELDS WITH APPLICATIONS TO DIELECTRIC BREAKDOWN

By L. A. BUTLER*

[Manuscript received November 11, 1966]

Summary

The method of images is used to compute the field between a charged sphere and an earthed plane. From this field distribution the electrical conductivity of a sphere-plane system and also the temperature distribution during thermal breakdown are determined for ranges of geometrical and electrical parameters. Heat-sink efficiencies of the electrodes are included in the calculation, and an experimental method for assessing these is proposed.

I. INTRODUCTION

In many investigations of dielectrics at fields approaching the breakdown value the electrodes are a sphere and a plane. This geometry permits a single well-defined point of maximum field and gradual reduction of the field away from the point. The field lines are not accurately parallel at the axis of symmetry, but for sufficiently large sphere radius and small gap the approximation may be sufficiently accurate and the field intensity approximates that calculated from parallel-plane geometry. Frequently a connection is sought between pre-breakdown and breakdown phenomena, often involving pre-breakdown current. Current densities are usually measured using plane-parallel specimens to give a definable area of conduction with small edge effects. This difference in geometry between breakdown and pre-breakdown specimens complicates the connection sought. It is suggested that some problems may be resolved by computing the conductivity from sphere-plane measurements and using the same specimen for breakdown.

At higher temperatures (Hanscomb 1962) the initial electrical conductivity of alkali halides is sufficient to give rise to Joule heating, with consequent cumulative increase of conductivity and temperature. The basic equation of heat generation and conduction in a material in which an electric field is established is (O'Dwyer 1960)

$$\sigma F^2 = C_v \, dT/dt - K_1 \nabla^2 T, \quad (1)$$

where σ is electrical conductivity, F is electric field (magnitude), C_v is specific heat at constant volume, T is temperature, t is time, and K_1 is thermal conductivity. Hitherto this equation has not been solved for sphere-plane electrodes such as are used in experimental investigations.

II. CONDUCTIVITY CALCULATION

This computation involves solution of the field between a sphere and a plane. The analytical solution (e.g. Jeans 1948) involves awkward parameter changes and

* School of Physics, University of New South Wales, Kensington, N.S.W.

infinite series whose terms are not expressible in elementary functions. For numerical computations the method of images is suitable. It may be shown that the field between two spheres charged to equal and opposite potentials may be represented as being due to slowly converging infinite series of point charges inside the spheres. For spheres of equal radius the required sphere-plane field is that existing between one sphere and the plane of symmetry midway between the spheres.

From electrostatic theory (e.g. Pugh and Pugh 1960) recurrence relations for the charges and their locations have been derived, namely,

$$Q_1 = 4\pi\epsilon_0 R V, \quad (2)$$

$$D_1 = R + G, \quad (3)$$

$$Q_n = \frac{Q_{n-1} R}{D_1 + D_{n-1}} \quad n = 2, 3, 4, \dots, \quad (4)$$

$$D_n = D_1 - \frac{R^2}{D_1 + D_{n-1}} \quad n = 2, 3, 4, \dots, \quad (5)$$

where R is sphere radius, V is sphere potential, G is sphere-plane gap, and D is distance measured from the plane. Each Q_n has a corresponding charge $-Q_n$ situated at $-D_n$ in the image series.

We also introduce the parameter $B = R/G$. For most experimental work B lies in the range 10–1000. It is found that in this range D_n/D_{n-1} approaches unity monotonically from below. When D_n approximates D_{n-1} within the accuracy of the calculation the charges accumulate at a point given by

$$D_\infty = (2RG + G^2)^{1/2}. \quad (6)$$

(Approximation to 5 parts in 10^8 is given by $n = 20$ for $B = 10$ and by $n = 170$ for $B = 1000$.) The remaining Q_n are seen to form a geometric progression. Hence, a finite series of Q_n may be used, the last computed Q_n (say Q_k) being replaced with

$$Q'_k = \frac{Q_k}{1 - R(D_1 + D_\infty)^{-1}}. \quad (7)$$

The field at a point (s, z) may readily be computed in its components by summing the contributions from all the Q_n and $-Q_n$ (see Fig. 1).

Using the field components computed in this way the dielectric may be divided into cells having cylindrical symmetry and whose sides are always parallel to the local field. Twenty such cells were used (see Fig. 2). Conduction is assumed to be zero except through the area projected on the plane by the sphere; experimentally, a guard ring of radius R would be used. Assuming ohmic material fills the region between the sphere and the plane, resistances of the cells are computed by numerical integration. The vertical height of the increments is shown in Figure 2. Paralleling the cell resistances gives a resistance Z between the electrodes. (Conduction in the outer cells, however, considerably influences the value of Z (Fig. 3), and thus fairly accurate guard ring dimensions are needed.)

The resistance of a cylindrical slab of dielectric of radius R and thickness G is computed and divided into Z . A universal dimensionless factor C results which

depends only on B . Values of $C(B)$ are given in Table 1, together with ratios of conducting-region-of-sphere radius R_c (Fig. 2) to sphere radius R . Standard finite

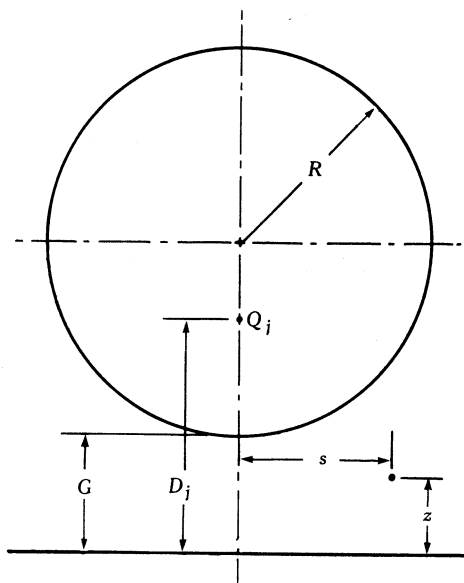


Fig. 1.—Geometry for determination of sphere-plane field due to point charges Q_j .

difference techniques (Hildebrand 1956) were used to interpolate 100 values of $C(B)$ and $\{C(B)\}^{-1}$ per decade of B on a log-log basis. Four-digit accuracy was obtained.

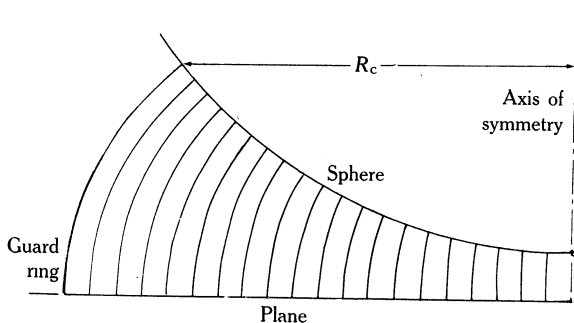


Fig. 2.—Cross section of dielectric-filled cells with sides parallel to the electric field. Cells are obtained by rotating the cross sections about the axis of symmetry. The size of intervals for numerical integration (conductivity calculation) and subcell size (breakdown calculation) is indicated by the horizontal lines to the right of the axis of symmetry. The guard ring defines the area of conduction from the plane.

For known values of sphere radius and gap the measured resistance of a sphere-plane system needs only to be divided by $C(B)$ to give the resistance of an equivalent disk of dielectric of radius R and thickness G . The conductivity of the dielectric may then easily be found.

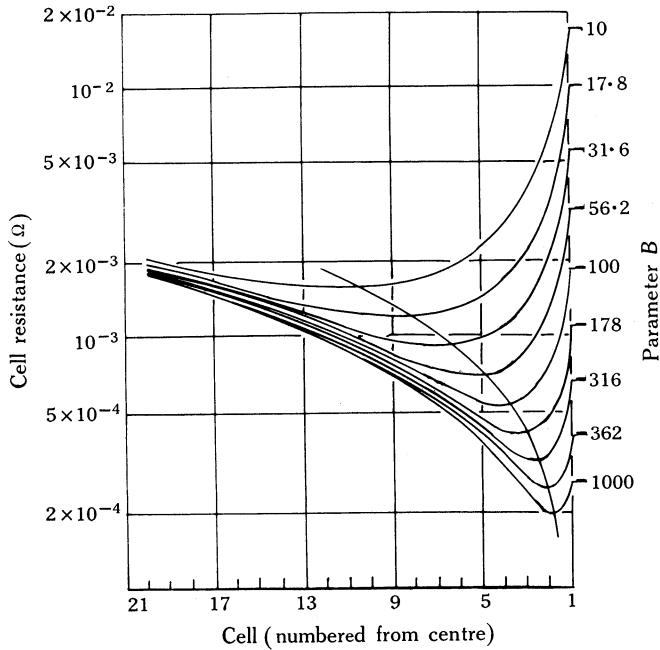


Fig. 3.—Resistance of cells as a function of cell “radius”. The minimum resistance is not at the axis of symmetry, and conduction is appreciable even at the radius of the guard ring. (Unit conductivity dielectric and sphere radius 1000 units assumed.)

TABLE I
UNIVERSAL DIMENSIONLESS SPHERE-PLANE CONDUCTIVITY FUNCTION $C(B)$
AND RATIO R_c/R

Log B	B	$C(B)$	R_c/R
1.00	10.000 000	3.202 993	0.768 336
1.25	17.782 794	4.390 906	0.779 465
1.50	31.622 777	6.277 883	0.785 766
1.75	56.234 133	9.304 461	0.789 322
2.00	100.000 000	14.143 108	0.791 324
2.25	177.827 943	21.914 279	0.792 451
2.50	316.227 769	34.714 341	0.793 084
2.75	562.341 332	55.441 690	0.793 439
3.00	1000.000 000	89.713 647	0.793 640

III. THERMAL BREAKDOWN CALCULATION

It is assumed for the solution of equation (1) that

- (i) $\sigma = \sigma_0 \exp(-\phi/kT)$, where σ_0 is constant, ϕ is activation energy, k is Boltzmann's constant, and T is temperature ($^{\circ}\text{K}$);
- (ii) F may be computed as for the conductivity calculation;
- (iii) C_v is constant over the temperature range;
- (iv) K_1 is constant over the temperature range;
- (v) $\nabla^2 T$ may be obtained by linear approximations to the differentials.

Assumption (i) may be justified empirically (e.g. Hanscomb 1962), as may assumption (iii) (e.g. Clusius, Goldman, and Perlde 1949). At high fields, space charge accumulation in the dielectric should be small in comparison with the charges on the electrodes, and (ii) is thereby justified. Experimental data for K_1 were not available above 100°C (McCarthy and Ballard 1960), but, as K_1 is reasonably constant above the Debye temperature of *c.* 7°C for NaCl, (iv) is the simplest extrapolation to make. For small cells (v) should introduce negligible error.

C_v is used rather than C_p as the small hot region is contained in the rest of the dielectric. Also C_p would have a stabilizing effect as it increases with temperature (J. R. Shepanski, personal communication).

Solution proceeds by dividing the dielectric into cells and subcells as for the conduction problem. Only the inner 12 cells are used as the outer cells remain at ambient temperature, a boundary condition justified by the small (*c.* 1 degC) temperature rises of the outermost cells used in the calculations.

Taking a small increment of time dt and using assumptions (i)–(v) the temperature rise dT for a subcell may be computed from equation (1). This is done for all subcells in the dielectric. Subcells adjacent to those in the dielectric but themselves inside the electrodes are then assigned temperature increments dT . These are calculated as $(1-S/100)$ times the difference between the temperature of the subcell and the temperature of the adjacent dielectric-filled subcell. Varying the parameter S between 0 and 100% allows simulation of different electrode heat-sink efficiencies. All these subcell temperature increments are stored in a matrix as they are computed.

Addition of this matrix to the subcell temperature matrix gives new values of temperature for all the subcells. A further time increment is now taken and the subcell temperatures computed again. If either a predetermined number of temperature increments have been computed, or if any cell has exceeded a predetermined temperature T_p , the temperature matrix is printed out. These printed matrices form a sequence analogous to the frames of a motion picture film, the last portion after T_p is exceeded being in "slow motion". Execution is terminated one increment after a predetermined melting temperature T_m is exceeded in any cell.

In order to make the programme as general as possible 18 parameters are read at execution time. These specify the voltage magnitude and waveform, specimen geometry, and thermal and electrical constants (including T_m , T_p , and the ambient temperature T_0) and print out controlling parameter, abnormal conditions parameters, electrode heat-sink efficiency S , and time increment dt .

Variation of all these parameters through wide ranges is impracticable. Fixed values (typical of NaCl) are used for all parameters except those varying in the investigation, as follows:

$$\begin{array}{ll}
 R = 4 \times 10^{-3} \text{ m}; & T_0 = 350^\circ\text{C}; \\
 G = 2 \times 10^{-4} \text{ m}; & T_p = 500^\circ\text{C}; \\
 C_v = 1.9 \times 10^6 \text{ J/m}^3; & T_m = 800^\circ\text{C}; \\
 K_1 = 5.0 \text{ W m}^{-1} (\text{degC})^{-1}; & S = 0\%; \\
 \phi = 1.0 \text{ eV}; & F = 0.25 \text{ MV/cm}; \\
 \sigma_0 = 2.5 \times 10^4 \text{ mho/m}; & dt = 2.0 \times 10^{-5} \text{ sec.}
 \end{array}$$

The temperature matrix was printed out every 50 increments. It was assumed, also, that the voltage pulse is instantaneously applied and constant thereafter until the temperature of the hottest part of the dielectric reaches the melting point.

TABLE 2
TIME TO BREAKDOWN t^* , AS A FUNCTION OF FIELD STRENGTH F^* AND CONDUCTIVITY σ , AND COMPUTED K VALUES ($K \equiv F^*(t^*\phi/\mathcal{R})^{1/2}$)

σ (mho/m)	\mathcal{R} (M Ω)	F^* (MV/cm)	t^* (msec)	K
1.0×10^5	0.054	0.5	0.104	0.69
		0.25	0.40	0.68
		0.1	2.48	0.68
2.5×10^4	0.216	1.0	0.11	0.71
		0.5	0.41	0.69
		0.25	1.64	0.69
		0.1	10.72	0.70
5.0×10^3	1.08	1.0	0.51	0.69
		0.5	2.12	0.70
		0.25	8.52	0.70

Using impulse thermal theory (O'Dwyer 1960) it may be shown that the peak voltage of a linearly rising transient is $\sqrt{3}$ times that of an instantaneously applied constant voltage giving the same time to breakdown t^* . Hence, when the thermal conduction term from (1) is small, the present results may be related to the experimental values of Hanscomb (1962) and of Butler and Hanscomb (1965), in which linearly rising transients were employed. It may be shown that (Butler and Hanscomb 1965), for impulse thermal breakdown with constant specimen geometry and ambient temperature, $K \equiv F^*(\phi t^*/\mathcal{R})^{1/2}$ is constant. F^* is the breakdown field strength (MV/cm), t^* is the time to breakdown (msec), ϕ is the activation energy for conduction (eV), and \mathcal{R} is the low-field specimen resistance (M Ω). K has a value of 1.5 for linearly rising transients and, hence, a value of 0.87 for constant voltage.

Computed K values (see Table 2) are seen to be constant for considerable variations in F^* and \mathcal{R} , as predicted by impulse thermal theory. This indicates that valid comparisons may be made with experiment as outlined above. The 20%

discrepancy between computed and experimental K values may be reconciled by the fact that no guard ring was used in the measurement of experimental \mathcal{R} values. Use of a guard ring would increase the experimental value of \mathcal{R} and hence decrease

TABLE 3
EFFECT OF ELECTRODE THERMAL SINK PARAMETER S ON TIME TO
BREAKDOWN t^*
With $S = 100\%$ and $F^* = 0.1$ MV/cm, thermal conditions are stable after
10 msec

F^* (MV/cm)	S (%)	t^* (msec)	K
0.5	0	0.41	0.69
	10	0.43	0.71
	31.6	0.46	0.73
	100	0.48	0.75
0.25	0	1.64	0.69
	10	1.69	0.70
	31.6	1.72	0.71
	100	1.98	0.76
0.1	0	10.72	0.70
	10	10.76	0.70
	31.6	10.86	0.71
	100	∞	∞

the experimental value of K . A value for $C(20) = 4.707$ has been used in the present conversion from conductivity to resistance, and this value depends on conduction from the plane being limited to the projected area of the sphere. Agreement is therefore considered to be adequate.

TABLE 4
EFFECT OF ϕ ON LOW-FIELD RESISTANCE \mathcal{R} AND TIME TO BREAKDOWN t^*

ϕ (eV)	\mathcal{R} (M Ω)	t^* (msec)	K
0.9	0.030	0.25	0.68
1.0	0.216	1.64	0.69
1.1	1.42	11.10	0.73

It is seen that the conduction of heat away into the specimen itself does not affect K greatly, and impulse thermal theory holds for times to breakdown less than 10 msec, when the electrodes absorb no heat. However, K is not constant, and the simple theory is not sufficient when the electrodes are good heat sinks and the time to breakdown is longer than a few milliseconds, as shown in Table 3. In the experimental work quoted above the electrodes were aluminium blocks. The higher values of K

TABLE 5
EFFECT OF SPECIMEN GEOMETRY ON SPECIMEN RESISTANCE \mathcal{R} AND TIME TO
BREAKDOWN t^*

Values $C(10) = 3.203$, $C(20) = 4.707$, and $C(50) = 8.573$ used

R (m)	\mathcal{R} (M Ω)	t^* (msec)	K
2.0×10^{-3}	0.588	1.68	0.42
4.0×10^{-3}	0.216	1.64	0.69
1.0×10^{-2}	0.063	1.70	1.30

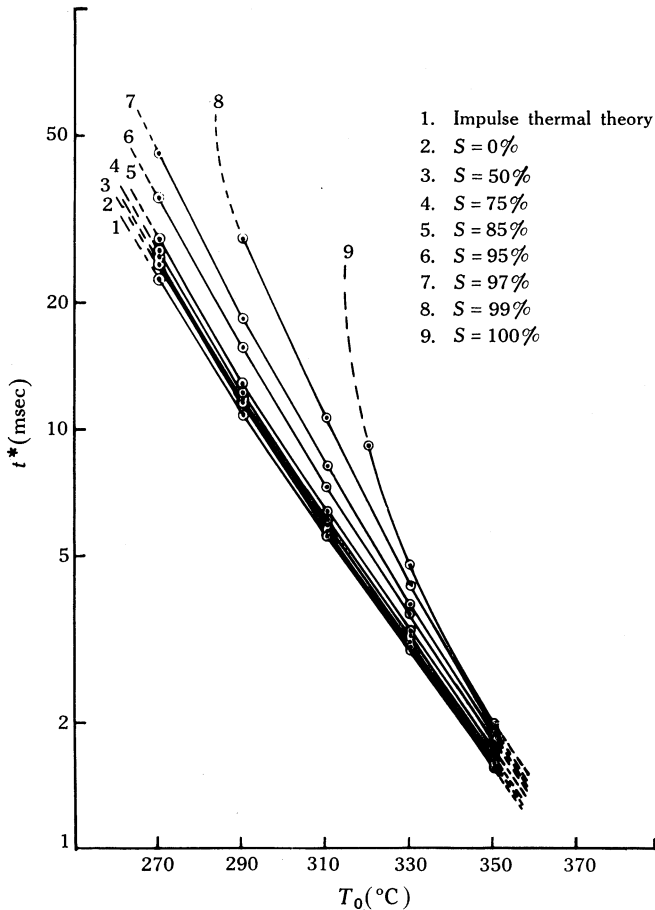


Fig. 4.—Time to breakdown t^* as a function of ambient temperature T_0 , for electrode heat-sink parameter (S) values between 0 and 100% and also as predicted by impulse thermal theory. Experimental S values may be determined by fitting experimental curves. Curves for $S = 99$ and 100% go to infinity, as stable thermal conditions ensued after 20 msec at the next lowest ambient temperature investigated.

associated with high S values are probably closest to the experimental conditions, and further reconciliation of computed and experimental K values is thereby effected.

Table 4 shows that, although changes in ϕ cause large changes in \mathcal{R} via the conductivity equation, the impulse thermal theory accounts fairly well for the resulting changes in t^* , as K is nearly constant. It has not been determined whether this is still true for large S values.

The spherical cavity in the NaCl specimens used in the experimental work quoted above was not accurately measured, being ground out and polished with a moist cloth lap. This uncertainty could help to reconcile the discrepancy between the experimental and computed K values (see Table 5). Although the resistance of the specimen (and with it, K) varies greatly the time to breakdown is nearly constant. These results suggest that specimen geometry is more important than has hitherto been supposed.

Impulse thermal theory predicts a variation of t^* with ambient temperature of the form

$$t^* = AT_0^2 \exp \phi k T_0, \quad (8)$$

where $A = C_v k / (F^{*2} \sigma_0 \phi)$. Computed curves of t^* as a function of T_0 for various values of S are shown in Figure 4. It is suggested that S may be determined experimentally from these curves, and work is proceeding along these lines.

With the exception of cases where steady thermal conditions were set up and no breakdown occurred, all these solutions of equation (1) showed similar features. For about the first 80% of the time to breakdown the temperature of the hottest cell rises linearly. After exceeding a value of approximately 450°C the temperature rises rapidly and quickly exceeds the melting point. Even if the time at which this occurs does not coincide with the time to breakdown the uncertainty in t^* is small, as invariably the last few cycles of computation show very rapid temperature changes in the hottest cells. The position of the hottest subcell is always on the axis of symmetry and does not vary during the solution. For $S = 0\%$ this subcell is at the sphere, where the field is most concentrated, and for $S = 100\%$ it is midway between the plane and the sphere.

The only cumbersome feature of the programme was that the maximum time increment dt that could be used was 20 μsec . Long time increments permitted some cells to "dissipate" more heat than was generated in them, resulting in negative temperatures. As reduction of dt below 20 μsec gave identical solutions this increment was used except for short times to breakdown. The criterion then was that at least 50 increments be used for solution.

Solutions required approximately 1 sec of execution time per time increment using an IBM 360/40 computer. Thus, 1 msec of "time to breakdown" may be simulated in 1 min of execution time. Values of t^* above about 25 msec, therefore, are impractical if extensive investigation of solutions is to be undertaken. Since the time to breakdown is less for a given value of F^* when a constant field is applied rather than a linearly rising pulse, it is suggested that this waveform be used when comparison with computed values is required.

IV. ACKNOWLEDGMENT

The author wishes to acknowledge helpful discussions with Mr. J. R. Shepanski.

V. REFERENCES

- BUTLER, L. A., and HANSCOMB, J. R. (1965).—*Aust. J. Phys.* **18**, 193–4.
CLUSIUS, K., GOLDMAN, J., and PERLIDE, A. (1949).—*Z. Naturf.* **A4**, 424.
HANSCOMB, J. R. (1962).—*Aust. J. Phys.* **15**, 504–12.
HILDEBRAND, F. B. (1956).—“Introduction to Numerical Analysis.” pp. 91–121. (McGraw-Hill: New York.)
JEANS, J. (1948).—“The Mathematical Theory of Electricity and Magnetism.” pp. 299–300. (Cambridge Univ. Press.)
MCCARTHY, K. A., and BALLARD, S. S. (1960).—*J. appl. Phys.* **31**, 31–5.
O'DWYER, J. J. (1960).—*Aust. J. Phys.* **13**, 270–7.
PUGH, E. M., and PUGH, E. W. (1960).—“Principles of Electricity and Magnetism.” pp. 102–4. (Addison-Wesley: Reading, Mass.)